Sensitive and Reversible Ammonia Gas Sensor Based on Single-Walled Carbon Nanotubes

Abniel Machín *, María Cotto, José Duconge, Carmen Morant, Florian I. Petrescu, Francisco Márquez *

Posted Date: 11 April 2023

doi: 10.20944/preprints202304.0211.v1

Keywords: ammonia; molybdenum disulfide; gold nanoparticles; CCVD.

Article

Sensitive and Reversible Ammonia Gas Sensor Based on Single-Walled Carbon Nanotubes

Abniel Machín [1,*], María Cotto [2], José Duconge [2], Carmen Morant [3], Florian I. Petrescu [2,4] and Francisco Márquez [2,*]

[1] Division of Natural Sciences, Technology and Environment, Universidad Ana G. Méndez-Cupey Campus, 00926PR, United States; machina1@uagm.edu

[2] Nanomaterials Research Group, Department of Natural Sciences and Technology, Division of Natural Sciences, Technology and Environment, Universidad Ana G. Méndez-Gurabo Campus, 00778PR, United States; mcotto48@uagm.edu (M.C.); jduconge@uagm.edu (J.D.)

[3] Department of Applied Physics, Autonomous University of Madrid and Instituto de Ciencia de Materiales Nicolás Cabrera, 28049, Spain; c.morant@uam.es

[4] IFToMM-ARoTMM, Bucharest Polytechnic University, Bucharest, (CE), Romania; fitpetrescu@gmail.com

* Correspondence: machina1@uagm.edu (A.M.); fmarquez@uagm.edu (F.M.)

Abstract: The present study reports on the fabrication and performance of ammonia sensors based on single-walled carbon nanotubes (SWCNTs) coated with gold nanoparticles (AuNPs). The AuNPs were incorporated onto the SWCNTs using two different methods: sputtering and chemical deposition. The sensors were exposed to controlled concentrations of ammonia at two temperatures, namely 25 °C and 140 °C, and their response was monitored through successive cycles of ammonia exposure (0.5 ppm and 1.0 ppm) and nitrogen purging. The results demonstrate that the sputtering-based deposition of AuNPs on SWCNTs led to the best sensor performance, characterized by a rapid increase in resistance values (t_{resp} = 12 s) upon exposure to ammonia and efficient recovery at 140 °C (t_{rec} = 52 s). By contrast, the sensor with chemically impregnated AuNPs exhibited a slower response time (t_{resp} = 25 s) and the same recovery time (t_{rec} = 52 s). Additionally, a novel device was developed that combined MoS_2-AuNPs (sputtering)-SWCNTs. This sensor was obtained by impregnating nano sheets of MoS_2 onto AuNPs (sputtering)-SWCNTs, and it showed improved sensor performance compared to the devices with only AuNPs. In this case, the sensor exhibited a better behavior, with a faster recovery of resistance values even at room temperature. Overall, the study provides valuable insights into the fabrication and optimization of SWCNT-based ammonia sensors for various applications, particularly in detecting and quantifying small amounts of ammonia (concentrations below 1 ppm).

Keywords: ammonia; molybdenum disulfide; gold nanoparticles; CCVD

1. Introduction

Ammonia, a colorless and toxic gas, is a versatile chemical with numerous industrial applications, including refrigeration, agriculture, pharmaceuticals, production of fertilizers, plastics, and power generation, among others [1–3]. The safe and effective use of ammonia requires accurate and reliable monitoring of its concentration in various environments. This is where sensors play a crucial role. In recent years, there has been significant progress in the development of sensors for the detection and measurement of ammonia [4–6]. However, the development of ammonia sensors that present high sensitivity and selectivity, and are capable of working at room temperature, is of special relevance. Exposure to ammonia, even at low concentrations, poses a significant risk to human health. To address this concern, the Occupational Safety and Health Administration (OSHA) has developed guidelines for maximum exposure times and dose limits in workplace environments where ammonia may be present [7]. The recommended maximum exposure time for workers is 8 hours, with a dose limit of approximately 25 parts per million (ppm) for an 8-hour workday. If the concentration of

ammonia exceeds this limit, then the recommended exposure time is much shorter. These guidelines aim to safeguard workers from the harmful effects of ammonia exposure, which can cause irritation of the eyes, nose, and throat, as well as respiratory difficulties, pulmonary edema, and in severe cases, even death. Compliance with these regulations is critical for maintaining a safe working environment and preventing the adverse health outcomes associated with ammonia exposure [7]. In this sense, different approaches have been developed using a long list of sensing materials to detect ammonia [8–12]. One popular type of sensor for ammonia detection is the electrochemical sensor [13]. These sensors rely on the detection of an electrochemical reaction to measure ammonia concentrations. They are well-known for their high sensitivity, fast response time, and the ability to perform real-time monitoring, making them a suitable choice for many industrial applications [13]. For instance, a study by Yavarinasab_et al. [14] describes the development of a polypyrrole-modified electrode for the electrochemical detection of ammonium ions in aqueous media. The sensor showed high selectivity and sensitivity for ammonium ions, with a detection limit of 2 ppm. Another study by Veluswamy et al. [15] describes sono-synthesis of reduced graphene oxide (rGO), and its performance for ammonia vapor detection at room temperature, with a minimum detection limit of 1 ppm and a detection range from 1 ppm to 100 ppm.

Infrared sensors are another type of sensor used for ammonia detection [16]. These sensors detect ammonia through the absorption of infrared radiation. They are widely used due to their fast response time, sensitivity, and ease of use. For example, a mid-infrared laser-based absorption sensor was developed for in-situ and simultaneous detection of ammonia, water, and temperature [16]. This ammonia sensor showed a detection limit of 7 ppb [16]. In another research, a microfiber Bragg grating (MFBG) was used to detect ammonia gas directly with ultrahigh sensitivity and without the possible interference of volatile organic compounds [17].

Optical sensors are another type of sensor used for ammonia detection [18]. These sensors use the absorption or fluorescence of light to detect ammonia, making them highly selective and sensitive [19]. These sensors can also detect signals through changes in the light scattering pattern [20]. Maierhofer et al. described the development of optical ammonia sensors based on fluorescent aza-BODIPY dyes, suitable for environmental, bioprocess, and reaction monitoring, capable of detecting ammonia levels of the order of 1µg/L [21]. In another research, Lu et al. developed a sensor based on reversible color change of an indicator of bromothymol blue loaded in a porous glass membrane, induced by ammonia gas released from the alkalinized water sample [22]. In this case, the behavior of the detector was linear with concentrations below 0.2 mg/L, and with detection levels in the microgram range.

Other sensors are based on resistance changes of active materials exposed to gas [23,24]. In this sense, various sensors based on metal oxides have been developed, and which are generally characterized by their low cost and sensitivity [23,24]. Among these materials, it is worth highlighting In_2O_3, CuO, NiO, Fe_2O_3, or V_2O_5, among others, with different dimensions and morphologies [25]. In this regard, 3D-hierarchical n-ZnO/p-NiO heterostructures were used for the development of ammonia sensors. In this investigation, detection levels were reached in the ppb range, although high working temperatures were required [26]. In another investigation, an ammonia sensor based on V_2O_5 nanosheets was developed [27]. In this case, the sensor was able to work at room temperature, showing high sensitivity and low detection limit even in the presence of interfering gases such as methanol, ethanol and others. The use of other materials for the development of resistance sensors, such as single-walled carbon nanotubes (SWCNTs), has been described in different investigations. In general, pristine SWCNTs show low ammonia detection efficiencies, so this type of materials has been modified by incorporating metallic nanoparticles [28], polymers [29,30], or different nanostructures [31,32]. In other investigations, ammonia sensors have been developed based on the chemical modification of SWCNTs by functionalization with carboxylic acids [33]. The behavior observed in these materials was attributed to the formation of hydrogen bonds between the ammonia and the oxygen present on the surface of the functionalized nanotubes.

In general, different types of ammonia sensors have certain characteristics, and the selection of a sensor for a specific application will depend on factors such as sensitivity, required response time, measurement range, cost, and complexity.

In this research we have developed sensors based on hybrid structures, formed by SWCNTs grown vertically through a catalytic chemical vapor deposition (CCVD) process, using TiN-SiO_2-Si substrates as support. These materials were subsequently modified by incorporating Au nanoparticles and MoS_2 nanosheets. The different materials used for the fabrication of these heterostructures were characterized by electron microscopy (SEM/TEM), Raman spectroscopy, and X-ray photoelectron spectroscopy (XPS). The devices prepared from these materials were subjected to ammonia detection tests at room temperature and 140 ºC, with ammonia concentrations of 0.5 and 1 ppm, showing linear behavior.

2. Materials and Methods

2.1. Preparation of Substrates for SWCNTs Growth

Silicon wafers (100) from El-CAT Inc. were used as substrates. Substrates were cleaned with isopropyl alcohol and next dried in an oven at 70 °C before use. In order to obtain different thicknesses of SiO_2 on Si, the substrates were subjected to a heat treatment at 200 °C for 5, 10 and 15 min and under vacuum (10^{-3} mb). Under these treatment conditions, layers of thermal silicon oxide (SiO_2) of ca. 200, 320 and 440 nm, respectively, were obtained. These SiO_2@Si substrates were then coated with TiN by physical vapor deposition (PVD). For this, a TiN target was used. The deposition temperature used was 110 °C, with a deposition time of 30 min and a TiN thickness of ca. 60 nm. The obtained materials were then treated to obtain a specific pattern of alternative TiN and SiO_2 zones. For this, an ion gun (Ion Tech Inc., 600 V and 10^{-4} mb pressure) was used, using a micrometer-sized patterned mask.

SWNTs were grown using a catalytic process. For this, the substrates obtained, with alternating zones of TiN and SiO_2, were used as catalyst support. The catalyst consisted of a mixture of Co-Mo, deposited on the substrates by dip coating, using the following procedure: dilute solutions of $Co(CH_3COO)_2 \bullet 4H_2O$ and $Mo(CH_3COO)_2$ in absolute ethanol were used as catalyst sources. Normally, to prepare 100 mL of the corresponding acetate solution, 0.02 g of the Mo^{II} salt or 0.04 g of the Co^{II} salt was used. Both solutions were sonicated for 20 min and shaken for 2 h. Acetate solutions were kept in the dark to avoid photodecomposition. In a first step the substrates were immersed into the Mo^{II} acetate solution for 10 sec. and subsequently calcined in an oven in air at 673 K for 20 min. After that, the substrates were allowed to cool to room temperature and the dip-coating process was repeated using the Co^{II} acetate solution. The substrates were then re-calcined in an oven at 673 K for 20 min. As a result, organic compounds were removed from the surface, giving rise to metals (Co and Mo) in oxidized form. As it could already be verified in other investigations, the metals are deposited mainly in the zones corresponding to SiO_2, fundamentally due to the much more polar behavior of SiO_2 than TiN, which acts as a physical barrier.

2.2. Synthesis of SWCNTs-SiO_2-Si

The substrates obtained as described above were used for the growth of SWCNTs. For this, a homemade catalytic CVD equipment was used, composed of a three-entry system (see Figure 1). A cylindrical quartz reactor with an inner diameter of 25 mm and a length of 1 m was installed inside a tube furnace. Substrates in a ceramic boat were introduced within the quartz reactor. Next, the system was closed and evacuated to 10^{-2} Pa, by using a mechanical pump. After 15 min, the mechanical pump was stopped and a mixture consisting of 90% Ar and 10% H_2 gas was added to the reactor (300 sccm flow rate). Simultaneously, the reactor was heated up to 1173 K (10 $Kmin^{-1}$), which allowed the reduction of the Mo and Co oxides, giving rise to the appearance of Mo° and Co° nanoclusters, which are the true catalysts for the synthesis of SWNTs. Once the synthesis temperature was reached, the flow of Ar-H_2 was stopped and a mixture of 10% H_2 and 90% Ar with ethanol (99.5%) vaporized in the Ar current was introduced into the chamber, at a flow rate of 200 sccm. The ethanol introduced

Preprints (www.preprints.org) | NOT PEER-REVIEWED | Posted: 11 April 2023 doi:10.20944/preprints202304.0211.v1

was the carbon source for the synthesis of SWCNTs, for which a growth time of typically 5 min was used. The growth ended when the gas mixture was changed to Ar (300 sccm), and simultaneously the cooling of the furnace began.

2.3. Synthesis of Au@SWCNTs-SiO_2-Si

SWNTs grown according to the procedure described above were located exclusively on the areas corresponding to SiO_2. The presence of TiN, although it inhibits the growth of carbon nanotubes, is necessary to facilitate the growth of vertically organized SWCNTs in the more polar regions of SiO_2 (see Figure 2). SWNTs were then partially coated with Au using a sputtering system. The process was carried out under a vacuum of 5.10^{-2} mb and with a sputtering time of 20 sec. The material obtained (Au@SWCNTs-SiO_2/Si) was then subjected to a heat treatment at 400 °C in flowing Ar (300 sccm) for 15 min. The amount of gold deposited by this procedure was estimated at ca. 5% (% at), based on EDS measurements.

To study the influence of the type of impregnation of SWCNTs with gold on the behavior of the sensor, a new experiment was carried out in which the SWCNTs were impregnated with Au through a chemical process. This procedure consisted of incorporating 0.2 mL of the Au precursor (0.005 g of $HAuCl_4$ in 2 mL of water) on the Si substrate with SWCNTs grown on the surface (SWCNTs@Si). After 15 minutes, the substrate impregnated with the gold reagent was immersed in a $NaBH_4$ solution (10 mg in 10 mL of H_2O) and allowed to react for 20 min at room temperature. Subsequently, the substrate was extracted and immersed in deionized water (3 times) to remove the reducing agent. This process was repeated 3 times and, finally, the substrates were dried overnight in a vacuum oven at 60 °C. The amount of gold deposited by this chemical method was evaluated by EDS, and estimated to be ca. 4% (% at), being similar to the result obtained by sputtering deposition (5%).

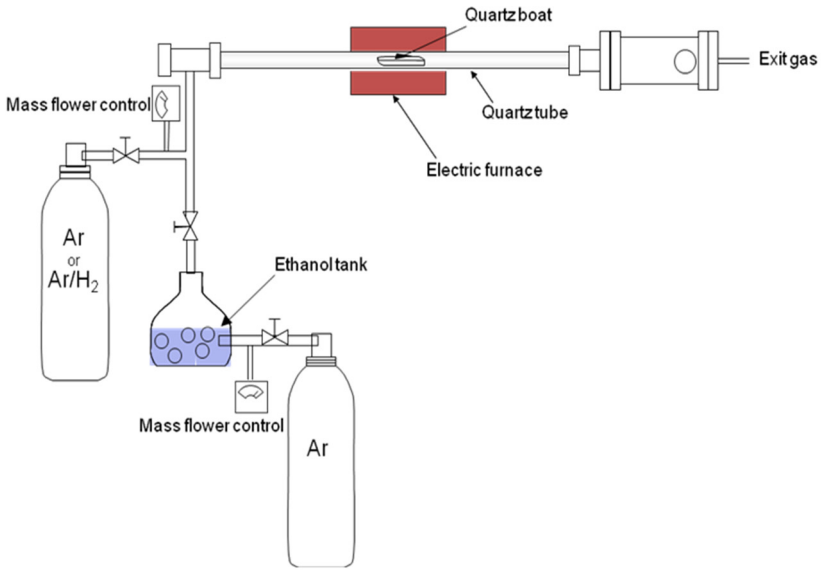

Figure 1. Diagram of the catalytic CVD system used for the growth of SWCNTs.

2.4. Synthesis of MoS_2-Au@SWCNTs-SiO_2-Si

MoS_2 nanosheets were incorporated onto Au@SWCNTs-SiO_2-Si, and their behavior in the detection of ammonia, was studied. To do this, commercial MoS_2 was subjected to an exfoliation process, which consisted of mixing 1 g of commercial MoS_2 with 50 mL of ethylenediamine. The mixture was kept under constant stirring for 48 h and then centrifuged to remove excess ethylenediamine. The solid obtained was redispersed in dimethylformamide and then sonicated for 3 h using a Tip Sonicator (Sonics Vibra-Cell VCX 750 Ultrasonic Processor) in pulsed mode (30% amplitude, pulse on 10 s, pulse off 10 s). Subsequently, the solution was left to rest for 4 hours, and

Preprints (www.preprints.org) | NOT PEER-REVIEWED | Posted: 11 April 2023 doi:10.20944/preprints202304.0211.v1

the supernatant was extracted and centrifuged for 30 min at 5000 rpm. Finally, the product was dried and sealed for later use.

The deposition of exfoliated MoS_2 on Au@SWCNTs-SiO_2-Si was carried out by impregnation, dispersing 20 mg of previously exfoliated MoS_2 nanosheets in 20 mL of ethanol. The mixture was sonicated for 1 hour using a Tip Sonicator (Sonics Vibra-Cell VCX 750 Ultrasonic Processor) in pulsed mode (10% amplitude, pulse on 5 s, pulse off 10 s). The Au@SWCNTs-SiO_2-Si substrates were immersed in this solution for 5 min. Subsequently, the substrates were extracted from the solution and placed in a deionized water bath, repeating this last process 3 times. The substrates were subsequently dried in a vacuum oven at 60 ºC overnight. The amount of MoS_2 deposited by this chemical impregnation method was evaluated by EDS analysis of Mo, and estimated to be ca. 6% (% at).

2.5. Characterization

The morphology of the materials was characterized by field emission scanning electron microscopy (FESEM) using a JEOL JSM-6010PLUS/LV, equipped with an INCA EDS XMAXN analyzer (Oxford Instruments, Abingdon, Oxfordshire, UK), and a FEI Verios 460L, equipped with a Quantax EDS Analyzer (Thermo Fisher Scientific, Hillsboro, Oregon, USA). Characterization by high-resolution transmission electron microscopy was carried out using a JEM 3000F microscope (JEOL, Peabody, MA, USA). Raman spectroscopy was carried out using a DXR Thermo Raman Microscope with a 532 nm laser source at 5mW power, and a resolution of 5 cm^{-1} (Waltham, MA, USA). X-Ray photoelectron spectroscopy (XPS), was carried out using a ESCALAB 220i-XL spectrometer with a non-monochromatic Mg Kα (1253.6 eV) radiation, operating at 20 mA and 12 kV (Waltham, MA, USA).

2.6. Target Gas Exposure

An in-house designed sensing chamber of 1 L capacity was used (see Scheme 1), capable of working at different temperatures through a thermostating system. The manufactured sensor was inserted into the chamber, with the terminals conveniently connected. The chamber was then evacuated to remove any possible contamination. For this, two vacuum pumps were used: one of them, to eliminate possible contamination in the gas lines, and an additional pump connected directly to the sensing chamber to remove any residual gas molecules. The system has an ammonia line (Gasco, 5 ppm ammonia diluted in nitrogen), and a second UHP nitrogen line (5.0). Both lines are connected to the sensing chamber, through flowmeters that allow controlled amounts of gas to be introduced. Resistivity measurements were carried out using a two-probe conductivity cell.

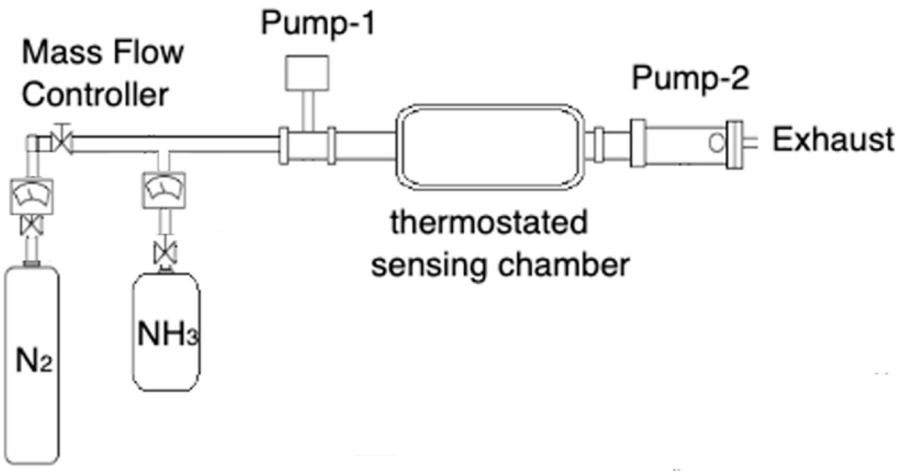

Figure 2. Schematic diagram of the setup for ammonia gas sensing.

Preprints (www.preprints.org) | NOT PEER-REVIEWED | Posted: 11 April 2023 doi:10.20944/preprints202304.0211.v1

3. Results and Discussion

3.1. Characterization of Nanomaterials

Figure 3 shows the SEM image of the different nanomaterials used in the manufacture of the different ammonia sensors developed in this research. Figure 3a shows the SEM image of vertically grown SWCNTs on TiN-SiO_2-Si substrates, on which Au nanoparticles have been deposited. SWCNTs are characterized by being grouped in bundles, whose diameter ranges between 10 and 15 nm (see below), and which are adhered to each other thanks to the presence of amorphous carbon. As can be seen, the distribution of Au nanoparticles is quite homogeneous, with diameters ranging between 5 and 8 nm. Figure 3b shows the SEM image of MoS_2 previously delaminated. As can be seen, delamination allowed obtaining structures of limited size, with average diameters below 200 nm. Figure 4 shows the HRTEM results of the different nanomaterials used. Figure 4a shows a bundle of SWCNTs. As can be seen, the fiber diameter is ca. 15 nm, and is formed by the grouping of individual SWCNTs, with an approximate diameter of 1.6 nm. These SWCNTs remain grouped forming these fibers thanks to the presence of an amorphous carbon that maintains their integrity. Similar results have already been observed previously [34]. Figure 4b shows a gold nanoparticle obtained by chemical synthesis. As observed, the nanoparticle shows a diameter of ca. 7 nm and is highly crystalline, whose interplanar spacing of ca. 0.23 nm has been indexed to (111) crystal plane of Au. Figure 4c presents the HRTEM image of MoS_2 that underwent ultrasonication-assisted exfoliation. The exfoliation process reveals the fine details of the atomic monolayer, as evident in the image. As previously reported in publications by our research group [35], MoS_2 exhibits a high degree of crystallinity, which is corroborated by the inset of Figure 4c. Additionally, the material also contains structural defects, which may potentially influence its properties and behavior.

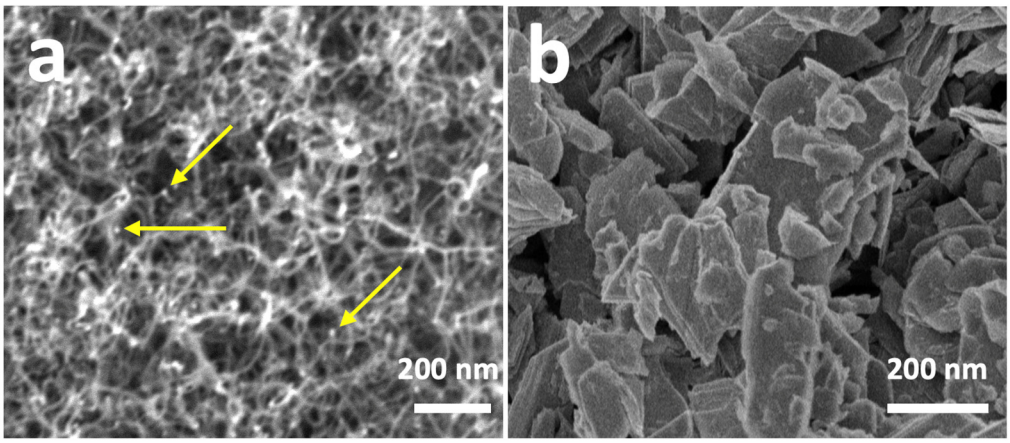

Figure 3. SEM micrographs of SWCNTs-AuNPs (**a**) and MoS_2 nanosheets (**b**). The arrows in Figure 3a indicate the presence of AuNPs.

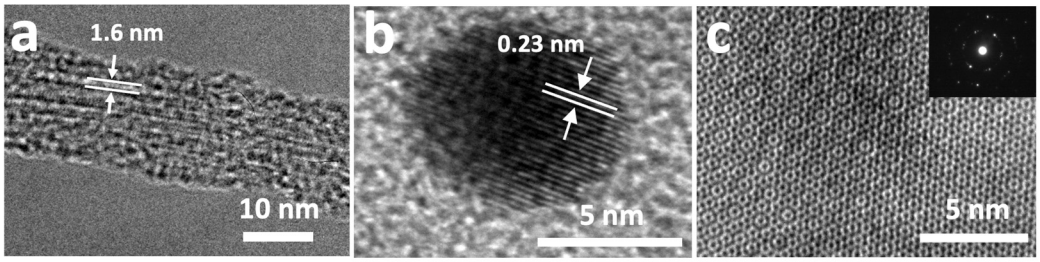

Figure 4. HR-TEM micrographs of the different components of the synthesized bundles of SWCNTs, showing the diameter of an isolated nanotube (**a**); Au NP, showing the characteristics of face-

Preprints (www.preprints.org) | NOT PEER-REVIEWED | Posted: 11 April 2023 doi:10.20944/preprints202304.0211.v1

centered-cubic (fcc) Au (111) (d = 0.23 nm) (**b**); and MoS_2 single layer with the corresponding selected area electron diffraction (SAED) pattern (**c**).

The different nanomaterials were also characterized by X-ray photoelectron spectroscopy (XPS). The transition corresponding to C1s (Figure 5a) is clearly asymmetric and has been deconvoluted into two components at ca. 285.5 eV and 287.4 eV. The most intense peak (284.6 eV) has been assigned to hybridized graphite-like carbon atoms (sp^2 carbon) [36], characteristic of the nanotube. The peak at 286.5 eV has been assigned to possible structural defects of SWCNTs, specifically to the presence of -C-O groups in the nanotube structure [36]. The presence of these defects in the nanotube is relevant, since they have the potential to serve as interaction zones with ammonia. Figure 5b shows the Au4f transition, with peaks at 83.4 eV and 86.9 eV, and a characteristic spin-orbit splitting of ca. 3.5 eV, typical of the presence of metallic gold [37]. Figure 5c shows the Mo3d and S2s transitions, corresponding to MoS_2. Mo3d shows two peaks at 232.0 eV and 228.9 eV, which have been attributed to the $Mo3d_{3/2}$ and $Mo3d_{5/2}$ doublet, respectively, and which have been assigned to the Mo^{4+} state I MoS_2 [37,38]. At 226.5 eV, a peak corresponding to the S2s transition, characteristic of MoS_2, is shown [37].

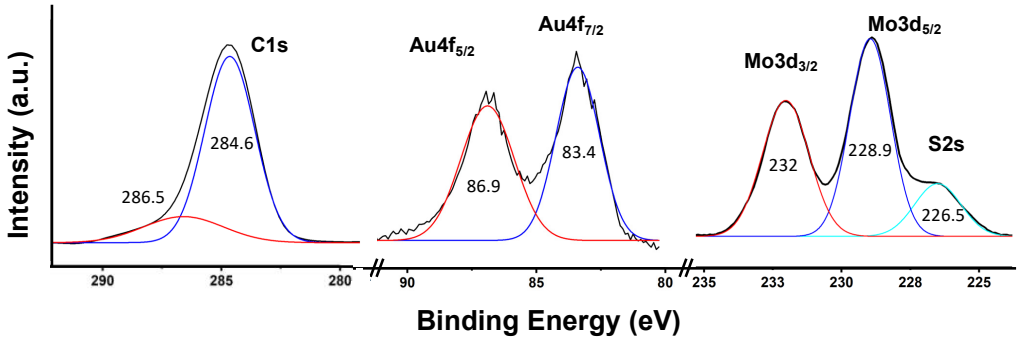

Figure 5. XPS core level spectra for C1s (a); Au4f (b); and Mo3d/S2s (c).

The different materials were characterized by Raman spectroscopy (Figure 6). Figure 6a corresponds to the Raman spectrum of SWCNTs grown by CCVD, after being detached from the substrate, showing an intense peak at 1594 cm^{-1} (G-band) , and a much less intense band (D-band) at ca. 1342 cm^{-1} [39]. Additionally, a band is observed at 2665 cm^{-1} (G'-band). The intensity ratio of the G/D bands is unequivocally related to the high purity of the SWCNTs. Below 300 cm^{-1} the RBM region is shown, whose position can be empirically correlated with the diameter of the nanotubes. For this, the formula $d = 284/\nu_{RBM}$ is used, where ν_{RBM} is the Raman shift corresponding to the RBM peak, and d is the diameter of the SWCNT (nm) [40]. The diameter determined by this approximation was 1.52 nm, which agrees with the dimensions determined by HRTEM (ca. 1.60 nm). Raman spectrum of MoS_2 (Figure 6b) is characterized by having two bands at 375 cm^{-1} and 404 cm^{-1} that have been assigned to the E^1_{2g} and A_{1g} modes, respectively [41]. The position of these bands varies with the level of exfoliation of the material, so these values indicate that exfoliation has led to the generation of MoS_2 nanosheets with few layers [42,43]. As observed in Figure 6c,d, the incorporation of gold nanoparticles (by sputtering) on the nanotubes did not produce apparent changes in the Raman spectrum. Figure 6d shows the Raman spectrum of the surface of the material subsequently used as a sensor (SWCNTs grown on TiN-SiO_2-Si substrate, with gold nanoparticles and MoS_2 nanosheets on the surface). As observed, the Raman spectrum shows two small peaks assigned to MoS_2 and one peak at ca. 550 cm^{-1} that is due to TiN, coming from the support.

Preprints (www.preprints.org) | NOT PEER-REVIEWED | Posted: 11 April 2023 doi:10.20944/preprints202304.0211.v1

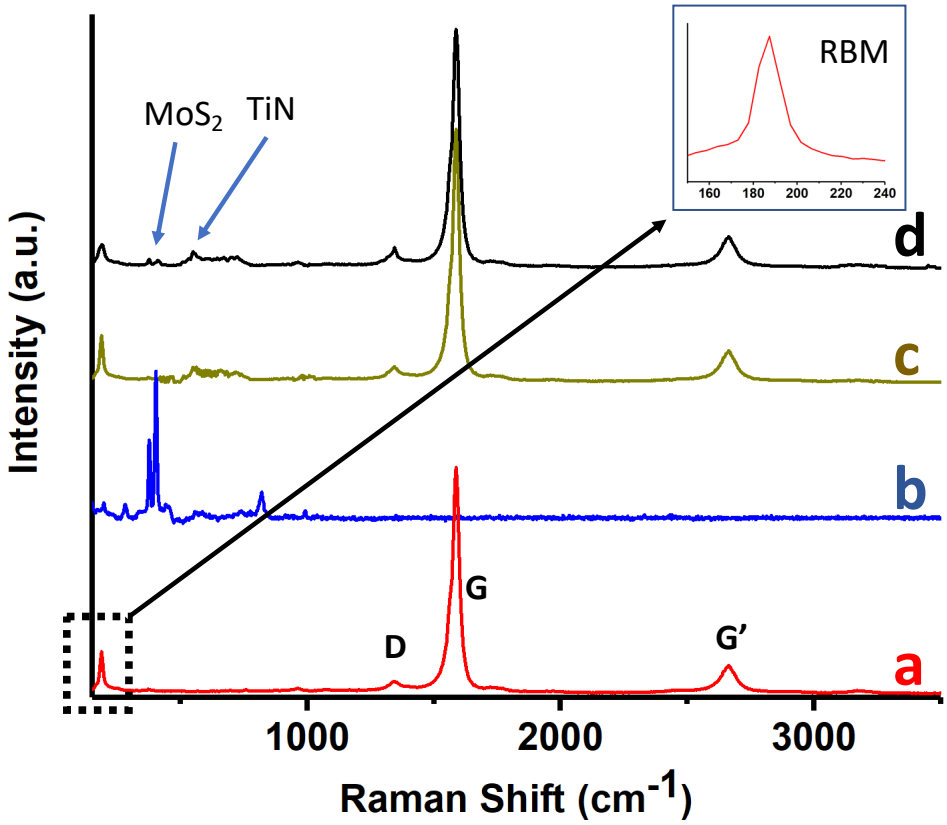

Figure 6. Raman spectra of as-synthesized SWCNTs (a); MoS_2 nanosheets (b); AuNPs-SWCNTs on TiN-SiO_2-Si substrates (c); and MoS_2-AuNPs-SWCNTs on TiN-SiO_2-Si substrates (d).

3.2. Assembly of the Device and Gas Sensing Properties

The manufacture of the ammonia sensors has been described in Section 2 (Materials and Methods). The different stages are summarized in Figure 7. As a result, three types of sensors were obtained: i) Au@SWCNTs, with AuNPs deposited by sputtering, ii) Au@SWCNTs, with AuNPs deposited by chemical impregnation and subsequent reduction, and iii) MoS_2-Au@SWCNTs, with AuNPs deposited by sputtering and MoS_2 by impregnation. The results obtained with sensors based on chemical impregnation of gold were less efficient than those obtained by sputtering, so the incorporation of MoS_2 was only performed in sensors with AuNPs deposited by sputtering. Figure 8 shows an image of the sensor based on lines of MoS_2-Au@SWCNTs, together with its schematic. The manufactured devices were tested by exposure to low concentrations of ammonia (0.5 ppm and 1 ppm). The measurements were carried out at two temperatures (25 °C and 140 °C), and using short cycles of exposure to ammonia and purge with nitrogen, for a total time of 90 min.

Preprints (www.preprints.org) | NOT PEER-REVIEWED | Posted: 11 April 2023 doi:10.20944/preprints202304.0211.v1

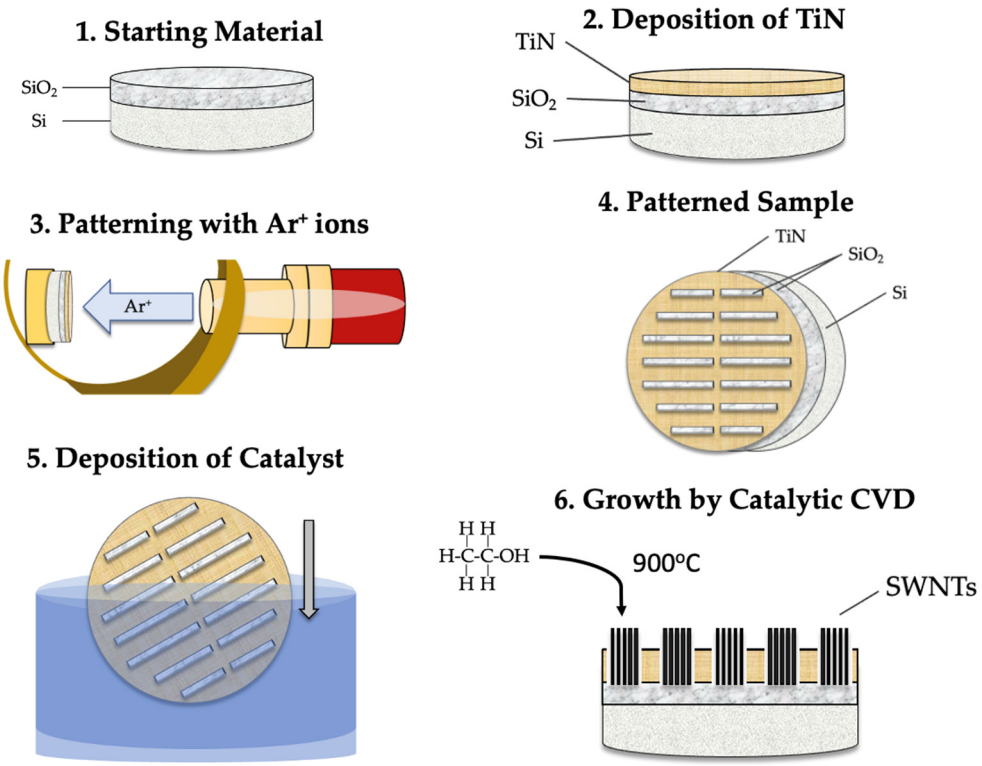

Figure 7. Schematic illustration of the substrate preparation process and the synthesis of SWCNTs: (i) Obtaining thermal SiO_2 (1); (ii) TiN deposition, and subsequent patterning of the substrate (2–4); (iii) Catalyst deposition (5); and (iv) Growth of SWCNTs by CCVD (6).

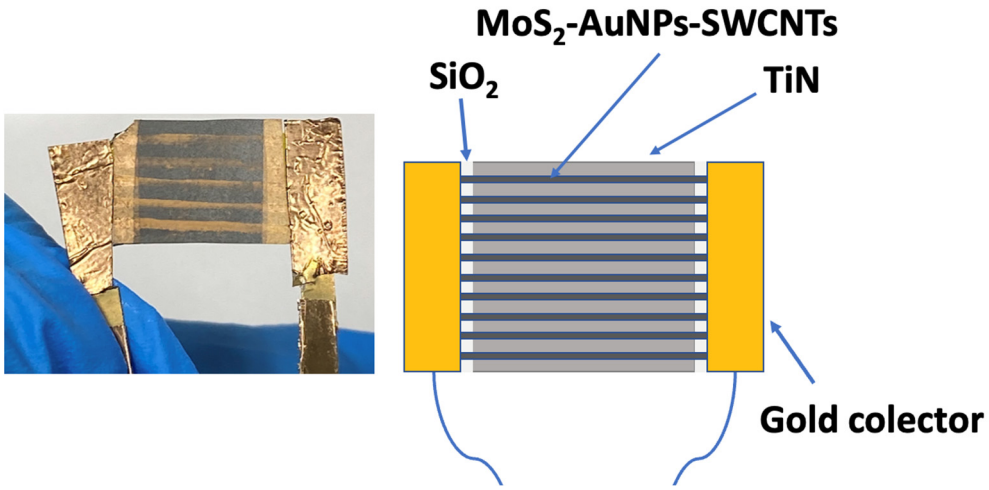

Figure 8. Picture of the devide based on MoS_2-Au@SWCNTs, and schematic illustration of the different components.

In this study, a single-walled carbon nanotube (SWNT)-based device with gold nanoparticles (AuNPs) deposited on its surface via sputtering (type-1) was exposed to controlled concentrations of ammonia dissolved in nitrogen, specifically 0.5 ppm and 1 ppm. The behavior of this sensor was analyzed at two different temperatures, 25 °C and 140 °C, using short cycles of ammonia input, followed by purging with nitrogen. The results of these experiments are presented in Figure 9. Notably, the response of the material was found to be consistent, with resistance values (R) that remained constant over the four cycles. At 25 °C (as shown in Figure 9a), a rapid increase in R was observed upon the introduction of ammonia. Even when the ammonia flow was terminated and the

Preprints (www.preprints.org) | NOT PEER-REVIEWED | Posted: 11 April 2023 doi:10.20944/preprints202304.0211.v1

detection chamber was purged with N_2, R did not fully return to its initial values. The observed effect of increasing resistance values (R) upon exposure to ammonia was found to become more pronounced throughout the multiple cycles studied. Interestingly, at a higher temperature of 140 °C, the recovery of R was more efficient. The results obtained at 25 °C may suggest that a portion of the ammonia that interacts with the sensor remains adsorbed on the surface even after purging with N_2. However, when the same process was carried out at a higher temperature (140 °C), the N_2 purge was found to be more effective, resulting in R values that almost returned to their initial values. The interaction energy between the sensor and ammonia could be responsible for this effect, requiring the use of high temperatures to promote the desorption of ammonia [44]. These findings were further supported by X-ray photoelectron spectroscopy (XPS) analysis (see Figure S1). Specifically, Figure S1 shows the spectra corresponding to N1s after ammonia adsorption on SWCNTs at 25 °C and 140 °C, followed by purging with N_2. As shown in Figure S1a, at 25 °C, a clear signal from ammonia was still observed. However, at 140 °C (Figure S1b), this signal was significantly reduced, indicating the more efficient removal of ammonia from the sensor surface. For comparative analysis, we contrasted the obtained results with those from a SWCNT-based sensor (without the presence of AuNPs). The outcomes are presented in Figure S2, demonstrating a less linear response with a considerably smaller change in R compared to the sensor with AuNPs. This justifies the necessity of incorporating AuNPs to enhance the device response. To further investigate the response of the AuNPs-SWCNTs based sensor, we conducted an extensive study with a single cycle of exposure to ammonia, as shown in Figure S3. The initial R value of the device before the exposure to ammonia was approximately 4.2 kΩ. Upon exposure to 1 ppm ammonia at 25 °C, a rapid increase in R was observed, peaking at approximately 4.6 kΩ. The response time (t_{resp}) was determined to be 12 s under the given conditions. Upon cessation of ammonia input and subsequent purging with N_2, the recovery time (t_{rec}) of R is approximately 52 s, although it does not attain the initial values, as evidenced in Figure 9. Figure S3 reveals that the recovered R value (ΔR) is approximately 19% greater than the initial R.

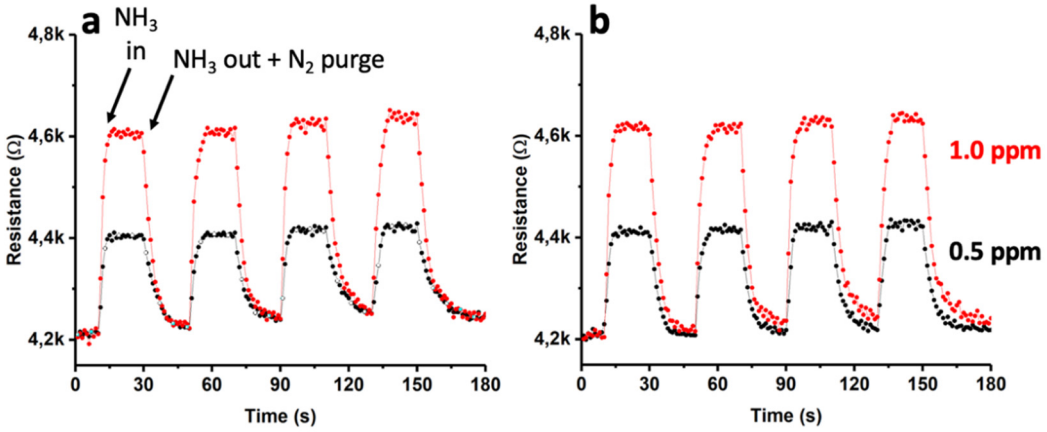

Figure 9. Dynamic response curve for the Au(sputtering)-SWCNTs composite gas sensor towards NH_3 (0.5 ppm and 1 ppm), at 25 °C (**a**) and 140 °C (**b**).

To investigate the impact of gold impregnation methods on the sensor behavior, a new experiment was conducted. Herein, AuNPs were deposited through a chemical impregnation and reduction process, as described in Section 2.3. Figure 10 depicts the outcomes achieved using this material under experimental conditions equivalent to those delineated earlier.

Preprints (www.preprints.org) | NOT PEER-REVIEWED | Posted: 11 April 2023 doi:10.20944/preprints202304.0211.v1

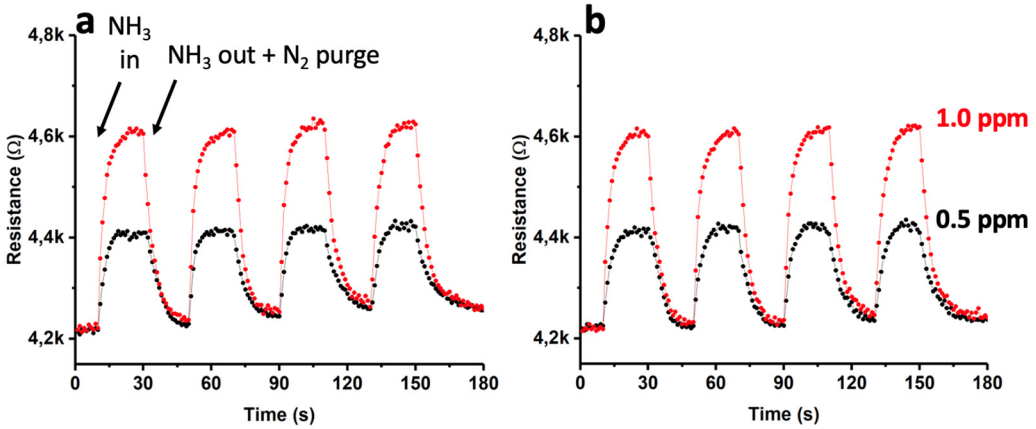

Figure 10. Dynamic response curves for the Au(chemical)-SWCNTs composite gas sensor towards NH_3 (0.5 ppm and 1 ppm), at 25 °C (**a**) and 140 °C (**b**).

As illustrated in Figure 10, the performance of this sensor exhibits a resemblance to that observed in the case of AuNPs deposition through sputtering. Nevertheless, the response times (t_{resp}) experience a significant increase, reaching nearly 25 seconds, which is twice that of the sensor fabricated via sputtering. Conversely, it is worth noting that the recovery of R, at both 25 °C and 140 °C, is similar to that observed in a sensor produced by sputtering.

Based on the outcomes obtained using different materials, and considering that the sensor exhibiting the best performance was obtained through AuNPs deposition by sputtering, a novel device was prepared using MoS_2-Au(sputtering)-SWCNTs. To achieve this, a fresh material composed of Au(sputtering)-SWCNTs was generated, and subsequently, MoS_2 was incorporated onto it, following the procedure delineated in Section 2.5. Subsequently, this device underwent identical ammonia exposure trials, and the findings are illustrated in Figure 11.

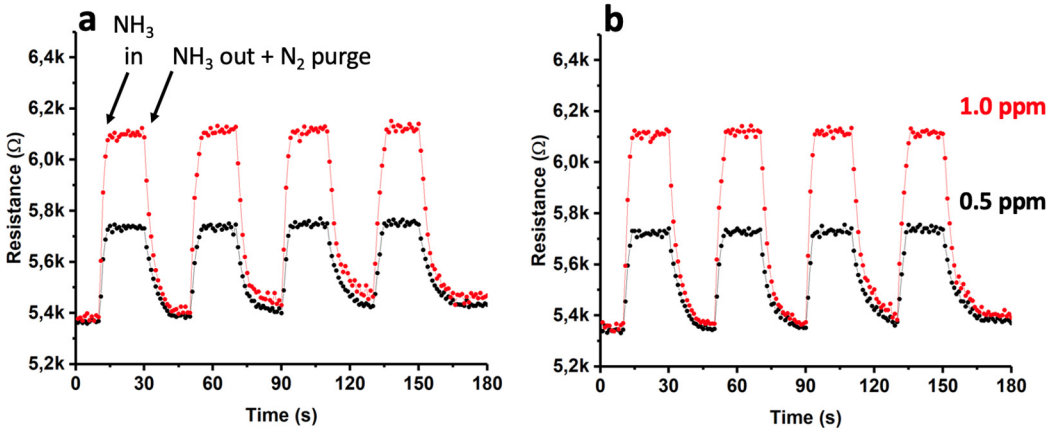

Figure 11. Dynamic response curves for the MoS_2-Au(sputtering)-SWCNTs composite gas sensor towards NH_3 (0.5 ppm and 1 ppm), at 25 °C (**a**) and 140 °C (**b**).

In this study, it can be observed that the trend of the sensor under analysis is similar to that of other sensors that have been previously analyzed. At a temperature of 25 °C, the retention of ammonia is still evident, leading to the fact that the sensor does not recover its previous values. However, at a temperature of 140 °C, the recovery of the sensor is more efficient. Comparing the results of this sensor with those obtained in the absence of MoS_2, a greater stability and better behavior are observed, as shown in Figure 9. The reason for this behavior is still unclear, although it is initially suggested that both AuNPs and MoS_2 may have a potential effect on the flow and

Preprints (www.preprints.org) | NOT PEER-REVIEWED | Posted: 11 April 2023 doi:10.20944/preprints202304.0211.v1

movement of electrons throughout the device, which represent active zones for interaction with ammonia.

In order to study the behavior of the sensor based on MoS_2-Au(sputtering)-SWCNTs under alternating cycles of exposure to different concentrations of ammonia at 140 °C, an additional study was conducted (see Figure 12). As can be observed, the device performs efficiently at these concentrations, with a recovery of R similar to that observed in previous exposures.

Finally, the same device was subjected to increasing concentrations of ammonia to investigate the proportionality of the response (see Figure 13). The sensor was exposed to concentrations of 0.5, 1, 5, and 10 ppm. It can be observed that exposure to concentrations higher than those previously studied (e.g., 5 and 10 ppm) resulted in a clearly non-linear response, indicating device saturation. At an ammonia concentration of 25 ppm (not shown), the maximum resistance (R) measured did not surpass 7 kΩ, providing evidence of the device's saturation. The reason for this behavior could be attributed to the relatively low quantity of single-walled carbon nanotubes (SWCNTs) grown on the device lanes, which inevitably limits the sensor's practicality.

The results obtained in the present research are certainly relevant because they demonstrate the use of these sensors for detecting low concentrations of ammonia. Table 1 shows a state-of-the-art comparison of some of the most representative ammonia sensors developed in recent years. From the perspective of environmental sustainability, all components used in the development of these sensors are environmentally friendly. The gold nanoparticles, MoS_2, and Si have no environmental implications at the concentrations used. Additionally, the economic cost of these materials is minimal, even in the case of gold, since the amounts used for manufacturing are indeed negligible. This clearly represents a great advantage over other current or in-development sensors.

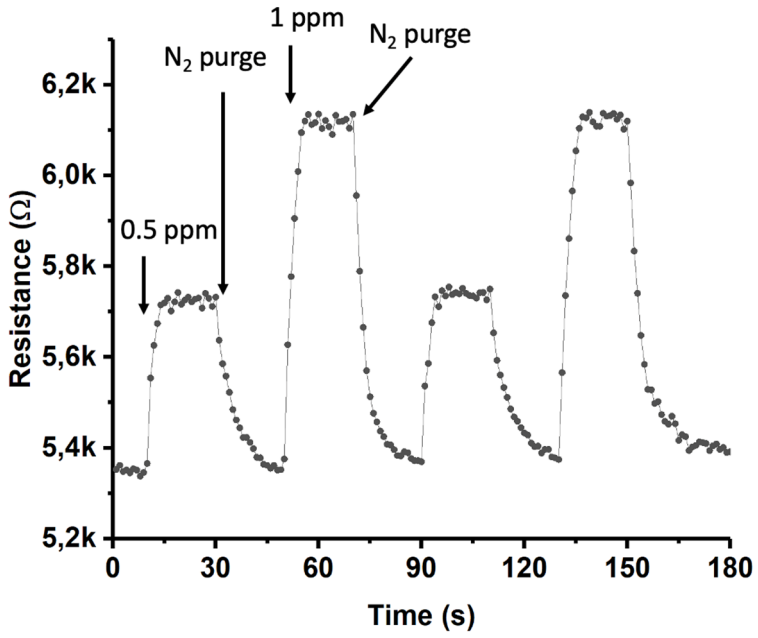

Figure 12. Dynamic response curves for the MoS_2-Au(sputtering)-SWCNTs composite gas sensor towards alternating exposure to NH_3 (0.5 ppm and 1 ppm), at 140 °C.

Preprints (www.preprints.org) | NOT PEER-REVIEWED | Posted: 11 April 2023 doi:10.20944/preprints202304.0211.v1

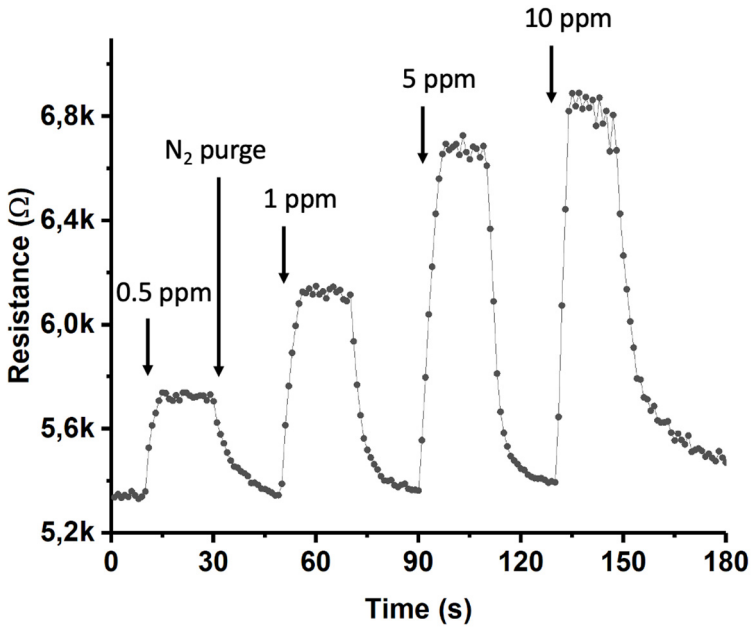

Figure 13. Dynamic response curves for the MoS_2-Au(sputtering)-SWCNTs composite gas sensor towards exposure to NH_3 (0.5, 1, 5 and 10 ppm), at 140 °C.

Table 1. Comparison of the results obtained in the present research with other ammonia sensors.

Sensing Material	Ammonia Detection Levels	Reference
Polypyrrole-modified electrode	0.5-5.0 ppm	[14]
Reduced Graphene Oxide (rGO)	1-100 ppm	[15]
Pd-doped ZnO	>5 ppm	[45]
Pd-SnO_2-rGO	5-150 ppm	[46]
Au-TiO_2	1-20 ppm	[47]
TiO_2	50 ppm	[48]
Bi_2Se_3/Bi_2O_3	5-180 ppm	[49]
Si	2-500 ppm	[50]
Ti_3C_2Tx-TiO_2	>200 ppb	[51]
CeO_2-ZnO	10-100 ppm	[52]
This research	0.5 ppm	N/A

4. Conclusions

In this study, several ammonia chemical sensors based on carbon nanotubes were developed. The carbon nanotubes were successfully synthesized on Si(100) substrates, which were coated with thermal SiO_2. The support was subsequently patterned to facilitate the growth of vertically aligned single-walled carbon nanotubes (SWCNTs) using a catalytic method. The resistance of the resulting composite materials, including those generated by deposition of AuNPs and MoS_2, was evaluated before and after exposure to ammonia. The sensitivity of the sensors was found to be temperature-dependent, with greater efficiency observed at 140 °C compared to 25 °C. However, the results indicate that the saturation of the sensor occurs at relatively low concentrations (above 1 ppm) for the devices manufactured, and the response at 5 and 10 ppm was clearly nonlinear, which could be

attributed to the limited number of SWCNTs grown in the devices. The results of this study show promise and provide the foundation for future research aimed at detecting trace amounts of ammonia in the ppb concentration range. Although the sensors developed in this study require several preparation steps, they are obtained easily, which could facilitate their potential application. The next phase of this research, which is already underway, will involve interconnecting several sensors, evaluating the selectivity of these sensors towards ammonia, and studying other factors that can significantly affect the device's sensitivity, such as humidity or the presence of other chemicals.

Supplementary Materials: The following supporting information can be downloaded at the website of this paper posted on Preprints.org. Figure S1**:** XPS transition of N1s from SWCNTs exposed to 1 ppm ammonia at 25 °C (a) and 140 °C (b), followed by N_2 purging; Figure S2: Dynamic response curve for SWCNTs towards NH_3 (0.5 ppm and 1 ppm), at 25 °C (a) and 140 °C (b); Figure S3: The response time and recovery time of the sensor based on Au-SWCNTs to an exposure of 1 ppm ammonia concentration at 25 °C.

Author Contributions: Conceptualization, F.M.; methodology, F.M., A.M.; formal analysis, F.M.; investigation, A.M., C.M., M.C., J.D., F.P.; resources, A.M., F.M., C.M., F.P.; writing—original draft preparation, F.M.; writing—review and editing, A.M., C.M., M.C., J.D., F.P.; supervision, F.M.; project administration, F.M.; funding acquisition, A.M., F.M., M.C., J.D., C.M., F.I.P. All authors have read and agreed to the published version of the manuscript.

Funding: Financial support from NSF Center for the Advancement of Wearable Technologies-CAWT (Grant 1849243), from the Consortium of Hybrid Resilient Energy Systems (DE-NA0003982), and from the Spanish Ministry of Economy and Competitiveness, under NanoCat-Com Project (PID2021-124667OB-I00), are gratefully acknowledged.

Institutional Review Board Statement: Not applicable for studies not involving humans or animals.

Informed Consent Statement: Not applicable for studies not involving humans.

Data Availability Statement: The data is contained in the article and is available from the corresponding authors on reasonable request.

Acknowledgments: The facilities provided by the National Center for Electron Microscopy at Complutense University of Madrid (Spain), by "Instituto de Micro y Nanotecnología IMN-CNM, CSIC, CEI UAM + CSIC" and by the Materials Characterization Center at University of Puerto Rico are gratefully acknowledged.

Conflicts of Interest: The authors declare no conflict of interest.

References

1. Li, X.; Li, X.; Li, Z.; Wang, J.; Zhang, J. WS_2 Nanoflakes Based Selective Ammonia Sensors at Room Temperature. *Sensors and Actuators B: Chemical* **2017**, *240*, 273–277, doi:10.1016/j.snb.2016.08.163.
2. Wang, Y.; Liu, J.; Cui, X.; Gao, Y.; Ma, J.; Sun, Y.; Sun, P.; Liu, F.; Liang, X.; Zhang, T.; et al. NH_3 Gas Sensing Performance Enhanced by Pt-Loaded on Mesoporous WO_3. *Sensors and Actuators B: Chemical* **2017**, *238*, 473–481, doi:10.1016/j.snb.2016.07.085.
3. Kanan, S.; El-Kadri, O.; Abu-Yousef, I.; Kanan, M. Semiconducting Metal Oxide Based Sensors for Selective Gas Pollutant Detection. *Sensors* **2009**, *9*, 8158–8196, doi:10.3390/s91008158.
4. Kwak, D.; Lei, Y.; Maric, R. Ammonia Gas Sensors: A Comprehensive Review. *Talanta* **2019**, *204*, 713–730, doi:10.1016/j.talanta.2019.06.034.
5. Verma, A.; Gupta, R.; Verma, A.S.; Kumar, T. A Review of Composite Conducting Polymer-Based Sensors for Detection of Industrial Waste Gases. *Sensors and Actuators Reports* **2023**, *5*, 100143, doi:10.1016/j.snr.2023.100143.
6. Baek, S.; Khazi, M.I.; Kim, J.-M. Colorimetric and Fluorometric Ammonia Sensor Based on Protonated Bipyridyl-Containing Polydiacetylene. *Dyes and Pigments* **2023**, *215*, 111254, doi:10.1016/j.dyepig.2023.111254.
7. *Toxic FAQ Sheet of Ammonia; Agency for Toxic Substances and Disease Registry (ATSDR), 2004; CAS 7664-41-7.*;
8. Tai, H.; Duan, Z.; He, Z.; Li, X.; Xu, J.; Liu, B.; Jiang, Y. Enhanced Ammonia Response of Ti_3C_2T Nanosheets Supported by TiO_2 Nanoparticles at Room Temperature. *Sensors and Actuators B: Chemical* **2019**, *298*, 126874, doi:10.1016/j.snb.2019.126874.
9. Tai, H.; Duan, Z.; Wang, Y.; Wang, S.; Jiang, Y. Paper-Based Sensors for Gas, Humidity, and Strain Detections: A Review. *ACS Appl. Mater. Interfaces* **2020**, *12*, 31037–31053, doi:10.1021/acsami.0c06435.

10. Panes-Ruiz, L.A.; Shaygan, M.; Fu, Y.; Liu, Y.; Khavrus, V.; Oswald, S.; Gemming, T.; Baraban, L.; Bezugly, V.; Cuniberti, G. Toward Highly Sensitive and Energy Efficient Ammonia Gas Detection with Modified Single-Walled Carbon Nanotubes at Room Temperature. *ACS Sens.* **2018**, *3*, 79–86, doi:10.1021/acssensors.7b00358.
11. Mackin, C.; Schroeder, V.; Zurutuza, A.; Su, C.; Kong, J.; Swager, T.M.; Palacios, T. Chemiresistive Graphene Sensors for Ammonia Detection. *ACS Appl. Mater. Interfaces* **2018**, *10*, 16169–16176, doi:10.1021/acsami.8b00853.
12. Tai, H.; Wang, S.; Duan, Z.; Jiang, Y. Evolution of Breath Analysis Based on Humidity and Gas Sensors: Potential and Challenges. *Sensors and Actuators B: Chemical* **2020**, *318*, 128104, doi:10.1016/j.snb.2020.128104.
13. Ryu, H.; Thompson, D.; Huang, Y.; Li, B.; Lei, Y. Electrochemical Sensors for Nitrogen Species: A Review. *Sensors and Actuators Reports* **2020**, *2*, 100022, doi:10.1016/j.snr.2020.100022.
14. Yavarinasab, A.; Janfaza, S.; Tahmooressi, H.; Ghazi, M.; Tasnim, N.; Hoorfar, M. A Selective Polypyrrole-Based Sub-ppm Impedimetric Sensor for the Detection of Dissolved Hydrogen Sulfide and Ammonia in a Mixture. *Journal of Hazardous Materials* **2021**, *416*, 125892, doi:10.1016/j.jhazmat.2021.125892.
15. Veluswamy, P.; Sathiyamoorthy, S.; P., S.; Karunakaran, G.; Lee, C.W.; Kuznetsov, D.; Kadarkaraithangam, J.; Ikeda, H. Sono-Synthesis Approach of Reduced Graphene Oxide for Ammonia Vapour Detection at Room Temperature. *Ultrasonics Sonochemistry* **2018**, *48*, 555–566, doi:10.1016/j.ultsonch.2018.07.012.
16. Ji, Y.; Duan, K.; Lu, Z.; Ren, W. Mid-Infrared Absorption Spectroscopic Sensor for Simultaneous and in-Situ Measurements of Ammonia, Water and Temperature. *Sensors and Actuators B: Chemical* **2022**, *371*, 132574, doi:10.1016/j.snb.2022.132574.
17. Fu, H.; Zhang, J.; Ding, J.; Wang, Q.; Li, H.; Shao, M.; Liu, Y.; Liu, Q.; Zhang, M.; Zhu, Y.; et al. Ultra Sensitive NH_3 Gas Detection Using Microfiber Bragg Grating. *Optics Communications* **2018**, *427*, 331–334, doi:10.1016/j.optcom.2018.06.059.
18. Passaro, V.; Dell'Olio, F.; De Leonardis, F. Ammonia Optical Sensing by Microring Resonators. *Sensors* **2007**, *7*, 2741–2749, doi:10.3390/s7112741.
19. Abdelaziz, O.A.; Abdallah, R.M.; Khater, R.A.; Abo Dena, A.S.; El-Sherbiny, I.M. Optical Ammonia-Sensing Probe Based on Surface-Plasmon Resonance of Silver-Nanoparticle-Decorated Superparamagnetic Dendritic Nanoparticles. *Plasmonics* **2023**, *18*, 201–212, doi:10.1007/s11468-022-01745-1.
20. Ahmed, S.; Park, Y.; Okuda, H.; Ono, S.; Korposh, S.; Lee, S.-W. Fabrication of Humidity-Resistant Optical Fiber Sensor for Ammonia Sensing Using Diazo Resin-Photocrosslinked Films with a Porphyrin-Polystyrene Binary Mixture. *Sensors* **2021**, *21*, 6176, doi:10.3390/s21186176.
21. Maierhofer, M.; Rieger, V.; Mayr, T. Optical Ammonia Sensors Based on Fluorescent Aza-BODIPY Dyes-a Flexible Toolbox. *Anal Bioanal Chem* **2020**, *412*, 7559–7567, doi:10.1007/s00216-020-02891-3.
22. Lu, D.; Qi, Z. Optical Ammonia-Nitrogen Sensor With Wide Dynamic Measurement Range. In Proceedings of the 2019 IEEE SENSORS; IEEE: Montreal, QC, Canada, October 2019; pp. 1–4.
23. Fernández-Ramos, M.D.; Capitán-Vallvey, L.F.; Pastrana-Martínez, L.M.; Morales-Torres, S.; Maldonado-Hódar, F.J. Chemoresistive NH_3 Gas Sensor at Room Temperature Based on the Carbon Gel-TiO_2 Nanocomposites. *Sensors and Actuators B: Chemical* **2022**, *368*, 132103, doi:10.1016/j.snb.2022.132103.
24. Nunes Simonetti, E.A.; Cardoso de Oliveira, T.; Enrico do Carmo Machado, Á.; Coutinho Silva, A.A.; Silva dos Santos, A.; de Simone Cividanes, L. TiO_2 as a Gas Sensor: The Novel Carbon Structures and Noble Metals as New Elements for Enhancing Sensitivity—A Review. *Ceramics International* **2021**, *47*, 17844–17876, doi:10.1016/j.ceramint.2021.03.189.
25. Pereira, P.F.M.; de Sousa Picciani, P.H.; Calado, V.; Tonon, R.V. Electrical Gas Sensors for Meat Freshness Assessment and Quality Monitoring: A Review. *Trends in Food Science & Technology* **2021**, *118*, 36–44, doi:10.1016/j.tifs.2021.08.036.
26. Zhao, Z.; Yang, H.; Wei, Z.; Xue, Y.; Sun, Y.; Zhang, W.; Li, P.; Gong, W.; Zhuiykov, S.; Hu, J. NH_3 Sensor Based on 3D Hierarchical Flower-Shaped n-ZnO/p-NiO Heterostructures Yields Outstanding Sensing Capabilities at Ppb Level. *Sensors* **2020**, *20*, 4754, doi:10.3390/s20174754.
27. Van Duy, L.; Nguyet, T.T.; Le, D.T.T.; Van Duy, N.; Nguyen, H.; Biasioli, F.; Tonezzer, M.; Di Natale, C.; Hoa, N.D. Room Temperature Ammonia Gas Sensor Based on P-Type-like V_2O_5 Nanosheets towards Food Spoilage Monitoring. *Nanomaterials* **2022**, *13*, 146, doi:10.3390/nano13010146.
28. Star, A.; Joshi, V.; Skarupo, S.; Thomas, D.; Gabriel, J.-C.P. Gas Sensor Array Based on Metal-Decorated Carbon Nanotubes. *J. Phys. Chem. B* **2006**, *110*, 21014–21020, doi:10.1021/jp064371z.
29. Datta, K.; Ghosh, P.; More, M.A.; Shirsat, M.D.; Mulchandani, A. Controlled Functionalization of Single-Walled Carbon Nanotubes for Enhanced Ammonia Sensing: A Comparative Study. *J. Phys. D: Appl. Phys.* **2012**, *45*, 355305, doi:10.1088/0022-3727/45/35/355305.
30. Chen, X.; Chen, X.; Ding, X.; Yu, X.; Yu, X. Enhanced Ammonia Sensitive Properties and Mechanism Research of PANI Modified with Hydroxylated Single-Walled Nanotubes. *Materials Chemistry and Physics* **2019**, *226*, 378–386, doi:10.1016/j.matchemphys.2019.01.061.

31. Mubeen, S.; Lai, M.; Zhang, T.; Lim, J.-H.; Mulchandani, A.; Deshusses, M.A.; Myung, N.V. Hybrid Tin Oxide-SWNT Nanostructures Based Gas Sensor. *Electrochimica Acta* **2013**, *92*, 484–490, doi:10.1016/j.electacta.2013.01.029.
32. Freddi, S.; Emelianov, A.V.; Bobrinetskiy, I.I.; Drera, G.; Pagliara, S.; Kopylova, D.S.; Chiesa, M.; Santini, G.; Mores, N.; Moscato, U.; et al. Development of a Sensing Array for Human Breath Analysis Based on SWCNT Layers Functionalized with Semiconductor Organic Molecules. *Adv. Healthcare Mater.* **2020**, *9*, 2000377, doi:10.1002/adhm.202000377.
33. Santra, S.; Sinha, A.K.; Ray, S.K. A Flexible Room Temperature Ammonia Sensor Based on Large Area, Transparent Single Wall Carbon Nanotube Thin Film. In Proceedings of the 2018 IEEE SENSORS; IEEE: New Delhi, October 2018; pp. 1–4.
34. Márquez, F.; López, V.; Morant, C.; Roque-Malherbe, R.; Domingo, C.; Elizalde, E.; Zamora, F. Structure and Characterization of Vertically Aligned Single-Walled Carbon Nanotube Bundles. *Journal of Nanomaterials* **2010**, *2010*, 1–7, doi:10.1155/2010/189214.
35. Fontánez, K.; García, D.; Ortiz, D.; Sampayo, P.; Hernández, L.; Cotto, M.; Ducongé, J.; Díaz, F.; Morant, C.; Petrescu, F.; et al. Biomimetic Catalysts Based on Au@TiO_2-MoS_2-CeO_2 Composites for the Production of Hydrogen by Water Splitting. *IJMS* **2022**, *24*, 363, doi:10.3390/ijms24010363.
36. Lee, Sun-Woo; Lee, Boong-Joo XPS Investigation and Field Emission Property of the Ar Plasma Processed Carbon Nanotube Films. *Transactions on Electrical and Electronic Materials* **2008**, *9*, 52–56, doi:10.4313/TEEM.2008.9.2.052.
37. Briggs, D.; Seah, M. *M. Practical Surface Analysis; Wiley:*; New York, NY, USA, 1994;
38. Ma, J.; Xing, M.; Yin, L.; San Hui, K.; Hui, K.N. Porous Hierarchical TiO_2/MoS_2/rGO Nanoflowers as Anode Material for Sodium Ion Batteries with High Capacity and Stability. *Applied Surface Science* **2021**, *536*, 147735, doi:10.1016/j.apsusc.2020.147735.
39. Park, Y.; Hembram, K.P.S.S.; Yoo, R.; Jang, B.; Lee, W.; Lee, S.-G.; Kim, J.-G.; Kim, Y.-I.; Moon, D.J.; Lee, J.-K.; et al. Reinterpretation of Single-Wall Carbon Nanotubes by Raman Spectroscopy. *J. Phys. Chem. C* **2019**, *123*, 14003–14009, doi:10.1021/acs.jpcc.9b02174.
40. Jorio, A.; Saito, R.; Hafner, J.H.; Lieber, C.M.; Hunter, M.; McClure, T.; Dresselhaus, G.; Dresselhaus, M.S. Structural (n,m) Determination of Isolated Single-Wall Carbon Nanotubes by Resonant Raman Scattering. *Phys. Rev. Lett.* **2001**, *86*, 1118–1121, doi:10.1103/PhysRevLett.86.1118.
41. Wieting, T.J.; Verble, J.L. Infrared and Raman Studies of Long-Wavelength Optical Phonons in Hexagonal MoS_2. *Phys. Rev. B* **1971**, *3*, 4286–4292, doi:10.1103/PhysRevB.3.4286.
42. Li, H.; Zhang, Q.; Yap, C.C.R.; Tay, B.K.; Edwin, T.H.T.; Olivier, A.; Baillargeat, D. From Bulk to Monolayer MoS_2: Evolution of Raman Scattering. *Adv. Funct. Mater.* **2012**, *22*, 1385–1390, doi:10.1002/adfm.201102111.
43. Castellanos-Gomez, A.; Quereda, J.; van der Meulen, H.P.; Agraït, N.; Rubio-Bollinger, G. Spatially Resolved Optical Absorption Spectroscopy of Single- and Few-Layer MoS_2 by Hyperspectral Imaging. *Nanotechnology* **2016**, *27*, 115705, doi:10.1088/0957-4484/27/11/115705.
44. Arshad, M.; Arshad, S.; Majeed, M.K.; Frueh, J.; Chang, C.; Bilal, I.; Niaz, S.I.; Khan, M.S.; Tariq, M.A.; Yasir Mehboob, M. Transition Metal-Decorated $Mg_{12}O_{12}$ Nanoclusters as Biosensors and Efficient Drug Carriers for the Metformin Anticancer Drug. *ACS Omega* **2023**, *8*, 11318–11325, doi:10.1021/acsomega.3c00058.
45. Zeng, Y.; Lou, Z.; Wang, L.; Zou, B.; Zhang, T.; Zheng, W.; Zou, G. Enhanced Ammonia Sensing Performances of Pd-Sensitized Flowerlike ZnO Nanostructure. *Sensors and Actuators B: Chemical* **2011**, *156*, 395–400, doi:10.1016/j.snb.2011.04.064.
46. Su, P.-G.; Yang, L.-Y. NH_3 Gas Sensor Based on Pd/SnO_2/rGO Ternary Composite Operated at Room-Temperature. *Sensors and Actuators B: Chemical* **2016**, *223*, 202–208, doi:10.1016/j.snb.2015.09.091.
47. Hwang, J.Y.; Lee, Y.; Lee, G.H.; Lee, S.Y.; Kim, H.-S.; Kim, S.; Park, H.J.; Kim, S.-J.; Lee, B.Z.; Choi, M.S.; et al. Room-Temperature Ammonia Gas Sensing via Au Nanoparticle-Decorated TiO_2 Nanosheets. *Discover Nano* **2023**, *18*, 47, doi:10.1186/s11671-023-03798-5.
48. Shooshtari, M.; Salehi, A. Ammonia Room-Temperature Gas Sensor Using Different TiO_2 Nanostructures. *J Mater Sci: Mater Electron* **2021**, *32*, 17371–17381, doi:10.1007/s10854-021-06269-8.
49. Das, B.; Riyajuddin, S.; Ghosh, K.; Ghosh, R. Room-Temperature Ammonia Detection Using Layered Bi_2Se_3/Bi_2O_3: A Next-Generation Sensor. *ACS Appl. Electron. Mater.* **2023**, *5*, 948–956, doi:10.1021/acsaelm.2c01496.
50. Le, Q.T.; Shikoh, A.S.; Kang, K.; Lee, J.; Kim, J. Room-Temperature Sub-Ppm Detection and Machine Learning-Based High-Accuracy Selective Analysis of Ammonia Gas Using Silicon Vertical Microwire Arrays. *ACS Appl. Electron. Mater.* **2023**, acsaelm.2c01383, doi:10.1021/acsaelm.2c01383.
51. Zhou, Y.; Wang, Y.; Wang, Y.; Yu, H.; Zhang, R.; Li, J.; Zang, Z.; Li, X. MXene $Ti_3C_2T_x$-Derived Nitrogen-Functionalized Heterophase TiO_2 Homojunctions for Room-Temperature Trace Ammonia Gas Sensing. *ACS Appl. Mater. Interfaces* **2021**, *13*, 56485–56497, doi:10.1021/acsami.1c17429.
52. Renganathan, B.; Rao, S.K.; Ganesan, A.R.; Deepak, A.; Kannapiran, N. Investigation of the Room Temperature Gas-Detecting Potential of CeO_2-Doped ZnO at Different Ratios Using Clad-Modified Fiber Optic Gas Sensor. *J Mater Sci: Mater Electron* **2022**, *33*, 23974–23985, doi:10.1007/s10854-022-08512-2.

 doi:10.20944/preprints202304.0211.v1